Effective action theory of Andreev level spectroscopy

Artem V. Galaktionov[1] and Andrei D. Zaikin[1,2]

[1]*I. E. Tamm Department of Theoretical Physics, P. N. Lebedev Physical Institute, 119991 Moscow, Russia*

[2]*Institute of Nanotechnology, Karlsruhe Institute of Technology (KIT), 76021 Karlsruhe, Germany*

(Received 22 October 2015; revised manuscript received 2 December 2015; published 16 December 2015)

With the aid of the Keldysh effective action technique we develop a microscopic theory describing Andreev level spectroscopy experiments in nontunnel superconducting contacts. We derive an effective impedance of such contacts which accounts for the presence of Andreev levels in the system. At subgap bias voltages and low temperatures, inelastic Cooper pair tunneling is accompanied by transitions between these levels resulting in a set of sharp current peaks. We evaluate the intensities of such peaks, establish their dependence on the external magnetic flux piercing the structure and estimate the thermal broadening of these peaks. We also specifically address the effect of capacitance renormalization in a nontunnel superconducting contact and its impact on both the positions and heights of the current peaks. At overgap bias voltages, the I-V curve is determined by quasiparticle tunneling and contains current steps related to the presence of discrete Andreev states in our system.

DOI: 10.1103/PhysRevB.92.214511 PACS number(s): 74.45.+c, 74.50.+r, 73.23.−b, 85.25.Cp

I. INTRODUCTION

The description of complex systems in terms of the so-called "collective" variables has a long history in condensed matter physics. An important example of such a variable is the "order parameter field" usually employed for the theoretical analysis of phase transitions. The convenience of this approach is guaranteed by its concise formulation, which, nevertheless, enables us to provide nontrivial results. Sometimes, the correct description can even be constructed phenomenologically, as was the case, e.g., with the celebrated Ginzburg-Landau theory of superconductivity [1] justified later on microscopic grounds [2].

Another milestone of this formalism is represented by the Feynman-Vernon influence functional theory [3] and the related Caldeira-Leggett analysis of quantum dissipation [4,5]. Within this description, all "unimportant" (bath) degrees of freedom are integrated out and the theory is formulated in terms of the effective action being the functional of the only collective variable of interest. Both dissipation and superconductivity are combined within the Ambegaokar-Eckern-Schön (AES) effective action approach [6,7] describing the macroscopic quantum behavior of metallic tunnel junctions. In this case, the collective variable of interest is the Josephson phase, and the whole analysis can be formulated for both superconducting and normal systems embracing various equilibrium and nonequilibrium situations.

Later on, it was realized that the AES type-of-approach can be extended to arbitrary (though sufficiently short) coherent conductors, including, e.g., diffusive metallic wires, highly transparent quantum contacts, etc. Also, in this general case, a complete effective action of the system can be derived both within Matsubara [8] and Keldysh [9] techniques, however, the resulting expressions turn out to be rather involved and usually become tractable only if one treats them approximately in certain limits. The character of approximations naturally depends on the problem under consideration. For example, Coulomb effects on the electron transport in short coherent conductors as well as on shot noise and higher current cumulants can be conveniently studied within the quasiclassical approximation for the phase variable [10–12], renormalization group methods [13], instanton technique [14], and for almost reflectionless scatterers [15,16]. Some of the above approximations are also helpful for the analysis of the frequency dispersion of current cumulants [16,17].

Another type of approximation is realized if one restricts the phase fluctuations to be sufficiently small. This approximation may be particularly useful for superconducting contacts with arbitrary transmission coefficients of their conducting channels. In this case, one can derive the effective action in a tractable form [18] and employ it for the analysis of various phenomena, such as, e.g., equilibrium supercurrent noise, fluctuation-induced capacitance renormalization, and Coulomb interaction effects.

An important feature of the effective action [18] is that it fully accounts for the presence of subgap Andreev bound states in superconducting contacts. In the case of sufficiently short contacts, the corresponding energies of such bound states are $\pm\epsilon_n(\chi)$, where

$$\epsilon_n(\chi) = \Delta\sqrt{1 - T_n \sin^2(\chi/2)}, \tag{1}$$

Δ is the superconducting gap, $T_n \leqslant 1$ defines the transmission coefficient of the n-th conducting channel, and χ is the superconducting phase jump across the contact. In the tunneling limit $T_n \ll 1$, we have $\epsilon_n(\chi) \simeq \Delta$ for any value of the phase χ, i.e., subgap bound states are practically irrelevant in this case. For this reason, such states are missing, e.g., in the AES action [6,7]. On the other hand, at higher values of transmission coefficients, the energies of Andreev levels (1) can be considerably lower than Δ and may even tend to zero for fully open channels and $\chi \approx \pi$. The presence of such subgap states may yield considerable changes in the behavior of (relatively) transparent superconducting contacts as compared to that of Josephson tunnel junctions.

Recently, the authors [19,20] performed experiments aimed at directly detecting Andreev levels by means of microwave spectroscopy of nontunnel superconducting atomic contacts. In this work, we will employ the effective action approach [18] and develop a microscopic theory of Andreev level

spectroscopy in superconducting contacts with arbitrary distribution of values of transmission coefficients T_n. As a result of our analysis, we will formulate a number of predictions which would allow for explicit experimental verification of our theory.

The structure of the paper is as follows. In Sec. II, we will specify the system under consideration and formulate the problem to be addressed in this work. In Sec. III, we will employ our effective action formalism [18] and evaluate the impedance of an effective environment formed by a system involving subgap Andreev levels. These results will then be used in Sec. IV in order to establish the $P(E)$-function for our system and to determine the relative intensity of different current peaks in the subgap part of the I-V curve. The effect of capacitance renormalization on both the positions and the heights of such peaks will be studied in Sec. V, while in Sec. VI, we will address thermal broadening of these peaks. In Sec. VII, we will analyze the I-V curve at larger voltages where quasiparticle tunneling dominates over that of Cooper pairs. The paper will be concluded in Sec. VIII by a brief summary of our main observations.

II. STATEMENT OF THE PROBLEM

Following the authors [19,20] we will consider the circuit depicted in Fig. 1. This circuit can be divided into two parts. The part to the right of the vertical dashed line represents a superconducting loop pierced by an external magnetic flux Φ. This loop includes a Josephson tunnel junction with normal state resistance R_N and Josephson coupling energy E_J connected to a nontunnel superconducting contact thereby forming an asymmetric SQUID. The latter contact is characterized by an arbitrary set of transmission coefficients T_n of its transport channels and—provided the superconducting phase difference χ is imposed—may conduct the

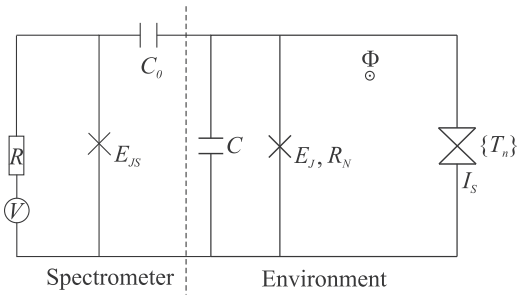

FIG. 1. The circuit under consideration. The measured system, shown to the right of the dashed line, represents an asymmetric SQUID comprising a Josephson tunnel junction with resistance R_N and Josephson coupling energy E_J and a nontunnel superconducting contact, characterized by an arbitrary set of transmission coefficients T_n of its conducting channels. The total capacitance C consists of a sum of geometric capacitances of both superconducting junctions C_Σ and also includes the renormalization term from the Josephson element, cf. Eq. (13) below. The superconducting loop is pierced by the magnetic flux Φ. The measuring device (the spectrometer) is shown to the left of the dashed line. It incorporates a voltage-biased tunnel junction with Josephson coupling energy E_{JS} connected to the measured system via a low resistance R and a large capacitance C_0.

supercurrent [21]

$$I_S(\chi) = \frac{e\Delta \sin\chi}{2} \sum_n \frac{T_n}{\sqrt{1 - T_n \sin^2(\chi/2)}} \times \tanh \frac{\Delta\sqrt{1 - T_n \sin^2(\chi/2)}}{2T}, \tag{2}$$

where $-e$ stands for the electron charge. Below, we will assume that temperature T is sufficiently low $T \ll \Delta$ and we will stick to the limit

$$R_N \ll R_c, \tag{3}$$

where $1/R_c = (e^2/\pi)\sum_n T_n$ is the normal state resistance of a nontunnel contact. In this case the critical current of the Josephson tunnel junction $\propto 1/R_N$ strongly exceeds that of the nontunnel superconducting contact $\propto 1/R_c$. In this limit, the phase jump across the Josephson junction is close to zero, while this jump across the nontunnel contact is $\chi \approx 2\pi\Phi/\Phi_0$. Here, $\Phi_0 = \pi c/e$ is the superconducting flux quantum, c is the light velocity and the Planck's constant is set equal to unity $\hbar = 1$.

The remaining part of the circuit in Fig. 1 (one to the left of the vertical dashed line) serves as measuring device called a spectrometer [20]. It consists of a voltage biased superconducting tunnel junction with Josephson coupling energy E_{JS} connected to the asymmetric SQUID via a large capacitance C_0.

Assuming that the value E_{JS} is sufficiently small, one can evaluate the inelastic Cooper pair current I across the spectrometer perturbatively in E_{JS}. At subgap values of the applied voltage V, one readily finds [22,23]

$$I = \frac{eE_{JS}^2}{2}[P(2eV) - P(-2eV)], \tag{4}$$

where

$$P(E) = \int_{-\infty}^{\infty} dt e^{iEt} \exp\left\{\frac{4e^2}{\pi}\int_0^\infty \frac{d\omega}{\omega}\mathrm{Re}[Z(\omega)] \times \left[\coth\frac{\omega}{2T}(\cos(\omega t) - 1) - i\sin(\omega t)\right]\right\} \tag{5}$$

is the function describing energy smearing of a tunneling Cooper pair due to its interaction with the electromagnetic environment characterized by a frequency-dependent impedance $Z(\omega)$ and temperature T. Provided the function $P(E)$ has the form of a delta function $P(E) \propto \delta(E - E_0)$, the current will be peaked as $I(V) \propto \delta(2eV - E_0)$. This situation is similar to a narrow spectral line on a photoplate, thereby justifying the name of the measuring device.

Coupling of the spectrometer to a single environmental mode (provided, e.g., by an LC circuit) was considered in Ref. [23]. In this case, the environmental impedance takes a simple form

$$Z_0(\omega) = \frac{i\omega}{C\left((\omega + i0)^2 - \omega_0^2\right)}. \tag{6}$$

Here, C is an effective capacitance of the LC circuit and ω_0 is the oscillation frequency. As usually, an infinitesimally small imaginary part $i0$ added to ω in the denominator indicates the retarded nature of the response. Employing Eq. (5) together

with the Sokhotsky's formula

$$\mathrm{Im}\,\frac{1}{x+i0} = -\pi\delta(x), \tag{7}$$

in the limit of low temperatures, one finds

$$P(E) = 2\pi e^{-\rho}\sum_{k=0}^{\infty}\frac{\rho^k}{k!}\delta(E-k\omega_0), \quad \rho = \frac{4E_C}{\omega_0}. \tag{8}$$

Here and below, $E_C = e^2/2C$ is the effective charging energy. Combining Eqs. (8) and (4) we obtain the I-V curve for our device which consists of narrow current peaks at voltages

$$2eV = k\omega_0, \quad k = 1,2,\ldots \tag{9}$$

The physics behind this result is transparent: a Cooper pair with energy $2eV$ that tunnels across the junction releases this energy by exciting the environmental modes. In the case of an environment with a single harmonic quantum mode considered above, this process can occur only at discrete set of voltages (9).

Turning back to the system depicted in Fig. 1, we observe a clear similarity to the above example of the LC circuit. Indeed, the asymmetric SQUID configuration on the right of Fig. 1 plays the role of an effective inelastic environment for the spectrometer. Bearing in mind the kinetic inductances of both the Josephson element and the nontunnel superconducting contact, to a certain approximation this environment can also be viewed as an effective LC circuit. An important difference with the latter, however, is the presence of extra quantum states—discrete Andreev levels (1)—inside the superconducting contact. Hence tunneling of a Cooper pair can also be accompanied by upward transitions between these states and—along with the current peaks at voltages (9)—one can now expect the appearance of extra peaks at

$$2eV = k\omega_0 + 2\epsilon_n(\chi), \quad k = 0,1,2,\ldots \tag{10}$$

This simple consideration served as a basic principle for the Andreev spectroscopy experiments [19] as well as for their interpretation [20]. While this phenomenological theory [20] correctly captures some important features of the phenomenon, it does not yet allow for the complete understanding of the system behavior, see, e.g., the corresponding discussion in Ref. [20]. Therefore the task at hand is to microscopically evaluate the function $P(E)$ for the asymmetric SQUID of Fig. 1, which governs the response of the spectrometer to the applied voltage. In the next section, we will describe the effective formalism which will be employed in order to accomplish this goal.

III. EFFECTIVE ACTION AND EFFECTIVE IMPEDANCE

Let us denote the total phase difference across the nontunnel superconducting contact as $\chi + 2\varphi(t)$, where χ is the constant part determined by the magnetic flux Φ and $2\varphi(t)$ is the fluctuating part of the superconducting phase. Assuming that the Josephson coupling energy of a tunnel junction E_J is sufficiently large one can restrict further analysis to small phase fluctuations $2\varphi(t) \ll 1$ in both tunnel and nontunnel contacts forming our asymmetric SQUID. The total action S describing our system consists of three terms

$$S = S_{\mathrm{Ch}} + S_J + S_{\mathrm{sc}}, \tag{11}$$

describing, respectively, the charging energy, the Josephson tunnel junction, and the nontunnel superconducting contact. In what follows, we will stick to the Keldysh representation of the action in which case it is necessary to consider the phase fluctuation variable on two branches of the Keldysh contour, i.e., to define $\varphi_1(t)$ and $\varphi_2(t)$. At subgap frequencies, the sum of the first two terms in Eq. (11) reads

$$S_{\mathrm{Ch}} + S_J = -\int dt\varphi_-(t)[\ddot{\varphi}_+(t)/(2E_C) + 4E_J\varphi_+(t)]. \tag{12}$$

Here, as usually, we introduced the so-called "classical" and "quantum" phases $\varphi_+(t) = (\varphi_1(t) + \varphi_2(t))/2$, $\varphi_-(t) = \varphi_1(t) - \varphi_2(t)$ and defined an effective capacitance

$$C = C_\Sigma + \frac{\pi}{16\Delta R_N}, \tag{13}$$

which accounts for the renormalization of the geometric capacitance C_Σ due to fluctuation effects in the Josephson junction [7]. The above expansion of the total effective action in powers of (small) phase fluctuations remains applicable for

$$E_J \gg E_C. \tag{14}$$

Expanding now the action S_{sc} around the phase value χ, we obtain [18]

$$iS_{\mathrm{sc}} = -\frac{i}{e}\int_0^t dt' I_S(\chi)\varphi_-(t') + iS_R - S_I, \tag{15}$$

where $I_S(\chi)$ is defined in Eq. (2) and

$$S_R = \int_0^t dt'\int_0^t dt''\mathcal{R}(t'-t'')\varphi_-(t')\varphi_+(t''), \tag{16}$$

$$S_I = \int_0^t dt'\int_0^t dt''\mathcal{I}(t'-t'')\varphi_-(t')\varphi_-(t''). \tag{17}$$

Both kernels $\mathcal{R}(t)$ and $\mathcal{I}(t)$ are real functions related to each other via the fluctuation-dissipation theorem. Defining the Fourier transform of these two kernels respectively as $\mathcal{R}_\omega = \mathcal{R}'_\omega + i\mathcal{R}''_\omega$ and $\mathcal{I}_\omega$ (having only the real part), we obtain

$$\mathcal{R}''_\omega = 2\mathcal{I}_\omega \tanh\frac{\omega}{2T}. \tag{18}$$

The action (15) results in the following current through the contact [18]

$$I = I_S(\chi) - e\int dt'\mathcal{R}(t-t')\varphi_+(t') + \delta I(t). \tag{19}$$

Here, $\delta I(t)$ is the stochastic component of the current. In the nonfluctuating case $\dot{\varphi}_+(t) = eV(t)$, and Eq. (19) defines the current-voltage relation.

The explicit expression for the kernel $\mathcal{R}(t)$ contains three contributions [18]: one of them originates from the subgap Andreev bound states, another one describes quasiparticle states above the gap and, finally, the third term accounts for the interference between the first two. As here we are merely interested in the subgap response of our system, below we will specify only the part of the kernel $\mathcal{R}$ governed by the Andreev

bound states. In the limit of low temperatures, it reads (cf. Eqs. (A3), (A5) in Ref. [18])

$$\mathcal{R}_\omega = \sum_n \frac{\gamma_n}{4\epsilon_n^2(\chi) - (\omega + i0)^2}, \tag{20}$$

where, as before, the summation is taken over the conducting channels of the superconducting contact and

$$\gamma_n = 4T_n^2(1-T_n)\frac{\Delta^4}{\epsilon_n(\chi)}\sin^4\frac{\chi}{2}\tanh\frac{\epsilon_n(\chi)}{2T}. \tag{21}$$

Now we are in a position to evaluate the current through the spectrometer. In the second order in $E_{\rm JS}$, we obtain

$$I(V) = \frac{eE_{\rm JS}^2}{2}\int dt\,\mathrm{Re}(e^{2ieVt}\langle e^{2i\varphi_1(t)-2i\varphi_1(0)} + e^{2i\varphi_2(t)-2i\varphi_1(0)} - e^{2i\varphi_1(t)-2i\varphi_2(0)} - e^{2i\varphi_2(t)-2i\varphi_2(0)}\rangle), \tag{22}$$

where the angular brackets imply averaging performed with the total Keldysh action (11). Under the approximations adopted here this average is Gaussian and it can be handled in a straightforward manner. As a result, we again arrive at Eqs. (4) and (5), where the inverse impedance of our effective environment takes the form

$$\frac{1}{Z(\omega)} = \frac{C(\omega^2-\omega_0^2)}{i\omega} + \sum_n \frac{e^2\gamma_n}{i\omega\left[4\epsilon_n^2(\chi)-\omega^2\right]}. \tag{23}$$

Here and below, $\omega_0 = \sqrt{8E_JE_C}$ is the Josephson plasma frequency.

Equation (23)—combined with Eqs. (1) and (21)—is our central result, which will be employed below in order to evaluate the $P(E)$ function and to quantitatively describe the results of Andreev level spectroscopy experiments.

IV. INTENSITY OF SPECTRAL LINES

It is obvious from Eqs. (4) and (5) that the positions of the current peaks are determined by zeros of the inverse impedance (23). Our theory allows to establish both the positions and relative heights of these peaks.

To begin with, let us assume that only one transport channel with transmission coefficient T_n in our superconducting contact is important, while all others do not exist or are irrelevant for some reason. In this case, from Eq. (23), we obtain

$$\mathrm{Re}[Z(\omega)] = \frac{\pi}{4C}\left\{\left[\delta(\omega-\sqrt{x_1})+\delta(\omega+\sqrt{x_1})\right]\left[1+\frac{4\epsilon_n^2(\chi)-\omega_0^2}{\sqrt{\left(4\epsilon_n^2(\chi)-\omega_0^2\right)^2+(4e^2\gamma_n/C)}}\right] + \left[\delta(\omega-\sqrt{x_2})+\delta(\omega+\sqrt{x_2})\right]\left[1+\frac{\omega_0^2-4\epsilon_n^2(\chi)}{\sqrt{\left(4\epsilon_n^2(\chi)-\omega_0^2\right)^2+(4e^2\gamma_n/C)}}\right]\right\}, \tag{24}$$

where

$$x_{1,2} = \frac{4\epsilon_n^2(\chi)+\omega_0^2 \mp \sqrt{\left(4\epsilon_n^2(\chi)-\omega_0^2\right)^2+4e^2\gamma_n/C}}{2}. \tag{25}$$

Outside of an immediate vicinity of the "level intersection" point $\omega_0 = 2\epsilon_n$, one can make use of the condition

$$\gamma_n \ll E_C\max\left(\omega_0^2,\epsilon_n^2(\chi)\right) \tag{26}$$

(which is typically well satisfied for the parameters under consideration) and expand the square roots in Eqs. (24) and (25) in powers of γ_n. As a result, one finds

$$\mathrm{Re}[Z(\omega)] = \frac{\pi}{2C}\left[\delta(\omega-\omega_0)+\delta(\omega+\omega_0)+\frac{2E_C\gamma_n}{\left(\omega_0^2-4\epsilon_n^2\right)^2}(\delta(\omega-2\epsilon_n)+\delta(\omega+2\epsilon_n))\right]. \tag{27}$$

Introducing the dimensionless expressions

$$\kappa_n = \frac{E_C\omega_0\gamma_n}{\epsilon_n\left(\omega_0^2-4\epsilon_n^2\right)^2}, \tag{28}$$

we get up to the first order in κ_n

$$P(E) = 2\pi e^{-\rho(1+\kappa_n)}\sum_{k=0}^{\infty}\frac{\rho^k}{k!}[\delta(E-k\omega_0)+\kappa_n\rho\delta(E-k\omega_0-2\epsilon_n)]. \tag{29}$$

Substituting this result into Eq. (4), we recover the I-V curve of our device at subgap voltages, which fully determines the heights of all current peaks.

For instance, Eq. (29) in combination with Eq. (4) yields the following ratio for the intensities of the two principal (voltage-integrated) current peaks occurring at the points $2eV = 2\epsilon_n$ and $2eV = \omega_0$:

$$\frac{\int_{eV\approx\epsilon_n} I(V)dV}{\int_{eV\approx\omega_0/2} I(V)dV} = \kappa_n \propto \frac{\sin^4\frac{\chi}{2}}{\epsilon_n^2(\chi)\left[\omega_0^2-4\epsilon_n^2(\chi)\right]^2}. \tag{30}$$

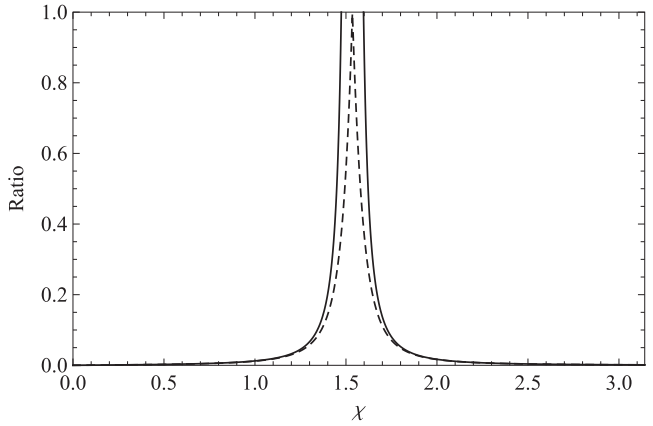

FIG. 2. The ratio of the intensities of the current peaks at $2eV = 2\epsilon_n$ and $2eV = \omega_0$. The parameters are $T_n = 0.9, \omega_0 = 1.48\Delta, e^2/C = 0.4\Delta$. The dashed line results from the exact expression (24), the solid line represents the approximate expression (30).

Here, the integration is performed over the voltage values in the immediate vicinity of the points $V = \epsilon_n/e$ and $V = \omega_0/2e$, respectively, in the numerator and in the denominator. Equation (30) determines relative intensities of the spectral lines as a function of the phase χ (or, equivalently, the applied magnetic flux Φ) and constitutes a specific prediction of our theory that can be directly verified in experiments. Equation (30) holds irrespective of the fact that in any realistic experiment the δ-function current peaks can be somewhat broadened by inelastic effects and it applies not too close to the point $\omega_0 = 2\epsilon_n$. This ratio of intensities is graphically illustrated in Figs. 2 and 3. The parameters of the figures are chosen in such a way that $\omega_0 = 2\epsilon_n$ at $\chi \approx \pi/2$. Figure 3 is characterized by the smaller value of γ_n. The approximate expression (30) provides a good description away from $\chi \approx \pi/2$ for both figures. It becomes better in Fig. 3, since it corresponds to smaller γ_n.

The above consideration can be generalized to the case of several conducting channels in a straightforward manner. For the sake of definiteness let us consider the contacts containing two transport channels with transmission coefficients T_n and T_m. In this case, Eq. (25) should be modified accordingly. Outside an immediate vicinity of the point $\omega_0 = 2\epsilon_n$, we obtain

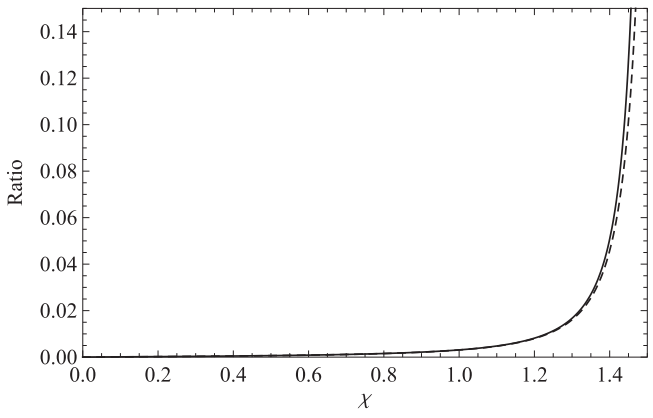

FIG. 3. The same as in Fig. 2 for $e^2/C = 0.1\Delta$.

the change of the root corresponding to the plasma mode

$$x_1 = \omega_0^2 + \frac{2E_C\gamma_n}{(\omega_0^2 - 4\epsilon_n^2)} + \frac{2E_C\gamma_m}{(\omega_0^2 - 4\epsilon_m^2)} + \ldots, \tag{31}$$

where ... stands for higher order in $\gamma_{n,m}$ terms. Similarly, for the other root, we get

$$x_2 = 4\epsilon_n^2 + \frac{2E_C\gamma_n}{(4\epsilon_n^2 - \omega_0^2)} - \frac{4E_C^2\gamma_n^2}{(4\epsilon_n^2 - \omega_0^2)^3} + \frac{E_C^2\gamma_n\gamma_m}{(4\epsilon_n^2 - \omega_0^2)^2(\epsilon_n^2 - \epsilon_m^2)} + \ldots. \tag{32}$$

It also follows that the coefficients in front of the δ functions in Eq. (27) take the same form in the leading order in $\gamma_{n,m}$. Thus, instead of Eq. (29), we now have

$$P(E) = 2\pi e^{-\rho(1+\kappa_n+\kappa_m)} \sum_{k=0}^{\infty} \frac{\rho^k}{k!}[\delta(E - k\omega_0) + \kappa_n\rho\delta(E - k\omega_0 - 2\epsilon_n) + \kappa_m\rho\delta(E - k\omega_0 - 2\epsilon_m)]. \tag{33}$$

Close to the intersection point between the plasma mode and one of the Andreev modes the picture will still be governed by Eqs. (24) and (25).

Thus Eq. (33) demonstrates that the two transport channels just yield "additive" contributions to the $P(E)$ function describing the asymmetric SQUID under consideration. Along the same lines, one can also recover the $P(E)$ function for the case of more than two transport channels available in the contact.

V. CAPACITANCE RENORMALIZATION

In the above analysis, we implicitly assumed that the Josephson plasma frequency ω_0 does not depend on χ. In the interesting for us limit (3), this assumption is well justified provided all transmission coefficients T_n remain substantially lower than unity. The situation may change, however, if at least one channel is (almost) open $T_n \approx 1$ and, on top of that, the phase χ controlled by the magnetic flux Φ is driven sufficiently close to π. In that case, capacitance renormalization effects due to phase fluctuations in the superconducting contact may yield an important contribution which needs to be properly accounted for.

In order to do so, we make use of the results [18] where the capacitance renormalization in a superconducting contact with arbitrary distribution of transmission coefficients T_n was investigated in details. Accordingly, Eq. (13) should in general be replaced by

$$C(\chi) = C_\Sigma + \frac{\pi}{16\Delta R_N} + \delta C(\chi), \tag{34}$$

where [18]

$$\delta C(\chi) = \frac{e^2}{4\Delta}\sum_n \left\{ \frac{2 - (2 - T_n)\sin^2(\chi/2)}{T_n \sin^4(\chi/2)} - (1 - T_n\sin^2(\chi/2))^{-5/2}\left[2T_n(T_n - 2)\sin^2(\chi/2) + 5 + T_n + \frac{2 - 2(1 + 2T_n)\sin^2(\chi/2)}{T_n\sin^4(\chi/2)}\right]\right\}. \tag{35}$$

For any distribution of transmission coefficients and small phase values $\chi \ll 1$, Eq. (35) yields

$$\delta C \simeq \frac{\pi}{16\Delta R_c}, \tag{36}$$

while for small $T_n \ll 1$ and any χ, one finds

$$\delta C(\chi) = \frac{3\pi}{32\Delta R_c}\left(1 - \frac{\cos\chi}{3}\right). \tag{37}$$

In both cases under the condition (3), an extra capacitance term $\delta C(\chi)$ in Eq. (34) can be safely neglected and the latter reduces back to Eq. (13). On the other hand, in the presence of highly transparent channels with $T_n \approx 1$, Eq. (35) results in a sharp peak of δC at $\chi \to \pi$:

$$\delta C \simeq \frac{e^2}{4\Delta}\sum_n \frac{1}{(1-T_n)^{3/2}}, \tag{38}$$

which, depending on the parameters, may even dominate the effective capacitance C at such values of χ. As a result, the plasma frequency ω_0 acquires the dependence on χ, which may become quite significant for phase values approaching $\chi \approx \pi$. In this case, in the results derived in the previous section, one should replace $\omega_0 \to \omega_0(\chi) = \sqrt{8E_J E_C(\chi)}$, where $E_C(\chi) = e^2/2[C + \delta C(\chi)]$.

The dependence $\delta C(\chi)$ for various distributions of transmission coefficients was studied in Ref. [18] (cf., e.g., Fig. 3 in that paper). One of the important special cases is that of diffusive barriers. In this case, the distribution of transmission coefficients T_n approaches the universal bimodal form with some channels being almost fully open and, hence, the capacitance renormalization effect should play a prominent role at $\chi \approx \pi$. At such values of χ, one finds [18] $\delta C(\chi) \simeq [\Delta R_c(\pi - \chi)^2]^{-1}$.

It should be emphasized that this capacitance renormalization influences not only the Andreev peaks at $eV = 2\epsilon_n$, but also the peaks occurring at voltages (9). Namely, as the phase χ approaches π, the positions of these peaks are shifted towards smaller voltages [since $\omega_0 \propto 1/\sqrt{C(\chi)}$], while the magnitudes of these peaks decrease [since $\rho \propto 1/\sqrt{C(\chi)}$]. Likewise, the magnitudes of principal Andreev peaks $\propto \rho\kappa_n$ may decrease significantly for $\chi \to \pi$.

VI. SPECTRAL LINEWIDTHS

Within the framework of our model, the width of current peaks should tend to zero at $T = 0$. However, at any nonzero T, these peaks become effectively broadened due to inelastic effects. The corresponding linewidth can be estimated as $\delta \sim 1/(\tilde{R}C)$, where $\tilde{R}(T)$ is the effective resistance of our system, which tends to infinity at $T \to 0$ but remains finite at nonzero temperatures. The value $\tilde{R}(T)$ is controlled by the imaginary part of the kernel $\mathcal{R}$. It is necessary to include two contributions to this kernel—one from the nontunnel superconducting contact (already discussed above) and another one from the Josephson tunnel junction. Accordingly, for the imaginary part of the Fourier component for the total kernel $\tilde{\mathcal{R}}$, we have

$$\tilde{\mathcal{R}}''_\omega = \mathcal{R}''_\omega + \mathcal{R}''_{J\omega}, \tag{39}$$

where (for $0 < \omega < 2\Delta$)

$$\mathcal{R}''_{J\omega} = \frac{1}{e^2 R_N}\int_\Delta^\infty \frac{d\epsilon[\epsilon(\epsilon+\omega)+\Delta^2]}{\sqrt{\epsilon^2-\Delta^2}\sqrt{(\epsilon+\omega)^2-\Delta^2}} \times\left(\tanh\frac{\epsilon+\omega}{2T} - \tanh\frac{\epsilon}{2T}\right) \tag{40}$$

and $\mathcal{R}''_\omega$ is obtained from Eq. (18) combined with Eq. (A1) from Ref. [18]. As a result, for the subgap region, we get

$$\mathcal{R}''_\omega = \sum_n \left\{ T_n^{3/2}\left[\tanh\frac{\omega+\epsilon_n(\chi)}{2T} - \tanh\frac{\epsilon_n(\chi)}{2T}\right]\theta(\omega-\Delta+\epsilon_n(\chi))\left|\sin\frac{\chi}{2}\right| \frac{\Delta(\omega\epsilon_n(\chi)+\Delta^2(1+\cos\chi))}{2\epsilon_n(\chi)((\omega+\epsilon_n(\chi))^2-\epsilon_n^2(\chi))}\sqrt{(\omega+\epsilon_n(\chi))^2-\Delta^2} + \frac{T_n}{\pi}\int_\Delta^\infty d\epsilon \frac{\sqrt{\epsilon^2-\Delta^2}\sqrt{(\epsilon+\omega)^2-\Delta^2}}{(\epsilon^2-\epsilon_n^2)((\epsilon+\omega)^2-\epsilon_n^2)}\left(\epsilon(\epsilon+\omega)+\Delta^2\cos\chi + T_n\Delta^2\sin^2\frac{\chi}{2}\right)\left(\tanh\frac{\epsilon+\omega}{2T} - \tanh\frac{\epsilon}{2T}\right)\right\}. \tag{41}$$

Note that in the lowest order in T_n this expression naturally reduces to that in Eq. (40) (with $R_N \to R_c$). On the other hand, for higher values of transmission coefficients the difference between the two contributions (40) and (41) become essential; while the former yields the standard thermal factor $\sim\exp(-\Delta/T)$, the latter turns out to be proportional to $\sum_n \exp(-\epsilon_n/T)$ (as long as $\omega + \epsilon_n > \Delta$).

It follows from the above consideration that the width of the plasma mode peak can be estimated as

$$\delta \sim \frac{2E_C\tilde{\mathcal{R}}''_{\omega_0}}{\omega_0}, \tag{42}$$

whereas the width of the current peak corresponding to the nth Andreev level (away from its intersection with the plasma mode) is

$$\delta \sim \frac{2\kappa_n E_C\tilde{\mathcal{R}}''_{2\epsilon_n}}{\omega_0} \tag{43}$$

with κ_n defined in Eq. (28). In the vicinity of the intersection point $\omega_0 = 2\epsilon_n$ it is necessary to replace κ_n by a more complicated expression resulting from Eq. (24).

These estimates demonstrate the crossover from the standard thermal broadening factor $\sim\exp(-\Delta/T)$ to a bigger one $\sim\exp(-\epsilon_n(\chi)/T)$ which accounts for the presence of subgap Andreev levels. Note that our present consideration is sufficient only in the absence of extra sources of dissipation and under the assumption of thermalization. Both additional dissipation and nonequilibrium effects can further broaden the current peaks beyond the above estimates. Nonequilibrium effects can be captured, e.g., within the effective action formalism [24] which—being equivalent to that of Ref. [18] in equilibrium—also allows for nonequilibrium population of Andreev bound states. The corresponding analysis, however, is beyond the frames of the present paper.

VII. QUASIPARTICLE CURRENT

To complete our analysis, let us briefly discuss the system behavior at higher voltages $eV > 2\Delta$. In this case, the I-V curve of our device is determined by quasiparticle tunneling. In the presence of an inelastic environment, one has [25]

$$I_{\rm qp}(V) = \int_{-\infty}^{\infty} \frac{d\omega}{2\pi} \frac{1-e^{-eV/T}}{1-e^{-\omega/T}} P(eV-\omega) I_{\rm qp}^{(0)}\left(\frac{\omega}{e}\right). \quad (44)$$

Here, $I_{\rm qp}(V)$ and $I_{\rm qp}^{(0)}$ represent the nonoscillating part of the voltage-dependent quasiparticle current, respectively, in the presence and in the absence of the environment. At $T \to 0$, the latter is defined by the well-known expression

$$I_{\rm qp}^{(0)}(V) = \frac{\Delta}{eR_{NS}} \theta(v-1)\left[2vE(1-v^{-2}) - \frac{1}{v}K(1-v^{-2})\right], \quad (45)$$

where R_{NS} is the normal resistance of the spectrometer junction, $v = eV/2\Delta$ and $E(k)$, $K(k)$ are complete elliptic integrals defined as

$$E(k) = \int_0^{\pi/2} d\phi \sqrt{1-k\sin^2\phi},$$
$$K(k) = \int_0^{\pi/2} \frac{d\phi}{\sqrt{1-k\sin^2\phi}}. \quad (46)$$

Combining Eqs. (44)–(46) with the expression for the $P(E)$ function [which is still defined by Eq. (29) with $\rho \to \rho/4 = E_C/\omega_0$] we arrive at the I-V curve, which contains two sets of current jumps (steps) at $eV = 2\Delta + k\omega_0$ and $eV = 2\Delta + k\omega_0 + 2\epsilon_n$. This behavior for an effective two mode environment is illustrated in Fig. 4, in which $P(E)$ is taken in the form

$$P(E) = 2\pi e^{-\rho_1-\rho_2} \sum_{k=0}^{\infty}\sum_{l=0}^{\infty} \frac{\rho_1^k}{k!}\frac{\rho_2^l}{l!}\delta(E-k\omega_1-l\omega_2). \quad (47)$$

VIII. CONCLUSIONS

In this work, we developed a microscopic theory enabling one to construct a quantitative description of microwave spectroscopy experiments aimed at detecting subgap Andreev states in nontunnel superconducting contacts. Employing the effective action analysis [18], we derived an effective impedance of an asymmetric SQUID structure of Fig. 1, which specifically accounts for the presence of Andreev levels in the system.

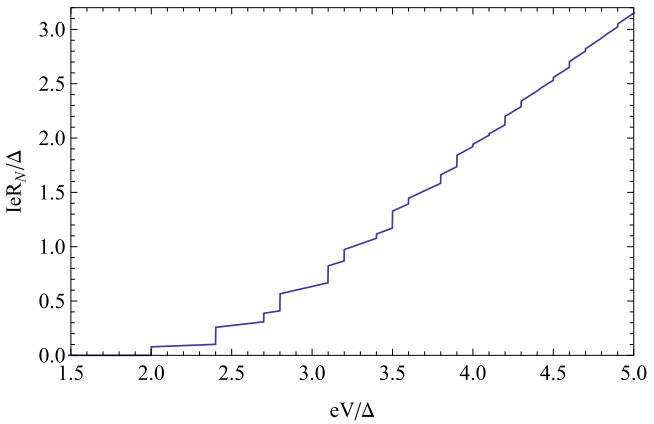

FIG. 4. (Color online) Zero-temperature quasiparticle current (44) with the environment characterized by two quantum modes with frequencies $\omega_1 = 0.4\Delta$ and $\omega_2 = 0.7\Delta$. We set $\rho_1 = 2$ and $\rho_2 = 1$. The current steps are observed at $eV = 2\Delta + k\omega_1 + l\omega_2$. If ρ_2 were much smaller than unity, $P(E)$ function (29) would be recovered and the steps would be observed at $eV = 2\Delta + k\omega_1$ and $eV = 2\Delta + k\omega_1 + \omega_2$.

At subgap voltages, the I-V curve for the spectrometer is determined by inelastic tunneling of Cooper pairs and has the form of narrow current peaks at voltage values (9) and (10). Our theory allows to explicitly evaluate the intensity of these current peaks and establish its dependence on the external magnetic flux Φ piercing the system. We also estimated thermal broadening of the current peaks to be determined by the factor $\sim \exp(-\epsilon_n(\chi)/T)$ rather than by the standard one $\sim \exp(-\Delta/T)$.

In the vicinity of the point $\Phi \approx \Phi_0/2$ and provided at least one of transmission coefficients T_n is sufficiently close to unity, the positions and heights of the current peaks may be significantly influenced by capacitance renormalization in a superconducting contact. For instance, the positions of the current peaks can decrease at the flux values $\Phi \approx \Phi_0/2$. We speculate that this effect could be responsible for experimental observations [19] of such a decrease in one of the samples (sample 3). This sample had about 20 conducting channels some of which could well turn out to be highly transparent, thus providing necessary conditions for substantial χ-dependent capacitance renormalization.

Finally, we also analyzed the system behavior at overgap voltages $eV > 2\Delta$ in which case the I-V curve is mainly determined by quasiparticle tunneling. The presence of both the plasma mode and Andreev levels results in the sets of current steps on the I-V curve of our device, as illustrated, e.g., in Fig. 4. All the above theoretical predictions can be directly verified in future experiments.

[1] V. L. Ginzburg and L. D. Landau, Zh. Eksp. Teor. Fiz. **20**, 1064 (1950).
[2] L. P. Gor'kov, Sov. Phys. JETP **36**, 1364 (1959).
[3] R. P. Feynman and A. R. Hibbs, *Quantum Mechanics and Path Integrals* (McGraw Hill, NY, 1965).
[4] A. O Caldeira and A. J Leggett, Ann. Phys. **149**, 374 (1983).
[5] U. Weiss, *Quantum Dissipative Systems*, 3rd ed. (World Scientific, Singapore, 2008).
[6] V. Ambegaokar, U. Eckern, and G. Schön, Phys. Rev. Lett. **48**, 1745 (1982).

[7] G. Schön and A. D. Zaikin, Phys. Rep. **198**, 237 (1990).
[8] A. D. Zaikin, Physica B **203**, 255 (1994).
[9] I. Snyman and Yu. V. Nazarov, Phys. Rev. B **77**, 165118 (2008).
[10] D. S. Golubev and A. D. Zaikin, Phys. Rev. Lett. **86**, 4887 (2001).
[11] A. V. Galaktionov, D. S. Golubev, and A. D. Zaikin, Phys. Rev. B **68**, 085317 (2003).
[12] A. V. Galaktionov and A. D. Zaikin, Phys. Rev. B **80**, 174527 (2009).
[13] D. A. Bagrets and Yu. V. Nazarov, Phys. Rev. Lett. **94**, 056801 (2005).
[14] Yu.V. Nazarov, Phys. Rev. Lett. **82**, 1245 (1999).
[15] I. Safi and H. Saleur, Phys. Rev. Lett. **93**, 126602 (2004).
[16] D. S. Golubev, A. V. Galaktionov, and A. D. Zaikin, Phys. Rev. B **72**, 205417 (2005).
[17] A. V. Galaktionov, D. S. Golubev, and A. D. Zaikin, Phys. Rev. B **68**, 235333 (2003).
[18] A. V. Galaktionov and A. D. Zaikin, Phys. Rev. B **82**, 184520 (2010).
[19] L. Bretheau, Ç. Ö. Girit, H. Pothier, D. Esteve, and C. Urbina, Nature (London) **499**, 312 (2013).
[20] L. Bretheau, Ç. Ö. Girit, M. Houzet, H. Pothier, D. Esteve, and C. Urbina, Phys. Rev. B **90**, 134506 (2014).
[21] I. O. Kulik and A. N. Omel'yanchuk, Fiz. Nizk. Temp. **4**, 296 (1978) [Sov. J. Low Temp. Phys. **4**, 142 (1978)]; W. Haberkorn, H. Knauer, and J. Richter, Phys. Stat. Solidi (A) **47**, K161 (1978); C. W. J. Beenakker, Phys. Rev. Lett. **67**, 3836 (1991).
[22] D. V. Averin, Yu. V. Nazarov, and A. A. Odintsov, Physica B **165-166**, 945 (1990).
[23] G.-L. Ingold and Yu. V. Nazarov, in *Single Charge Tunneling*, (Plenum Press, New York, 1992), Vol. 294, pp. 21–107.
[24] F. Kos, S. E. Nigg, and L. I. Glazman, Phys. Rev. B **87**, 174521 (2013).
[25] G. Falci, V. Bubanja, and G. Schön, Europhys. Lett. **16**, 109 (1991).